JOURNAL OF GEOPHYSICAL RESEARCH, VOL. 100, NO. B5, PAGES 8097–8114, MAY 10, 1995

Crustal structure of the Tuamotu Plateau, 15°S, and implications for its origin

Garrett Ito
MIT/WHOI Joint Program in Oceanography, Woods Hole Oceanographic Institution, Woods Hole, Massachusetts

Marcia McNutt
Department of Earth, Atmospheric, and Planetary Sciences, Massachusetts Institute of Technology, Cambridge

Richard L. Gibson
Earth Resources Laboratory, Department of Earth, Atmospheric, and Planetary Sciences
Massachusetts Institute of Technology, Cambridge

Abstract. We investigate the sedimentary and volcanic structure of the Tuamotu Plateau with multichannel seismic, seismic refraction, and gravity data along a ship track crossing the plateau near 15°S. The volcanic basement of the central portion of the plateau is capped with a 1 to 2-km-thick sediment layer composed of two compositional sequences. The uppermost sequence, with semblance-derived *P* wave velocities of 1.6-1.9 km/s and thicknesses of 0.2-0.9 km, is composed of pelagic sediments. The underlying sequence, with velocities 2.5-3.5 km/s and thicknesses of 0.5-1.5 km, is composed of limestone and volcaniclastic sediments. Sonobuoy refraction data show the upper 1 km of the volcanic basement to have velocities 4.5-5.5 km/s. The gravity data indicate that the platform is compensated by an elastic lithosphere with effective thickness 5±5 km and that the volcanic thickness is 9-10 km thicker than normal oceanic crust with a volume of $2.0\text{-}2.6 \times 10^6$ km^3. The inferred eruption rates of 0.1-0.13 km^3/yr are comparable to those of the Hawaiian and Marquesas island chains but substantially less than those of many oceanic plateaus. Radiometric and paleontological ages for the plateau and geomagnetic dates of the surrounding seafloor indicate that the northwestern portion of the plateau formed ~600 km off the axis of the paleo-Pacific-Farallon spreading center, on lithosphere of age ~10-20 Ma. Linear volcanic ridges and scarps bounding deep sediment-filled basins, however, are similar to features of oceanic plateaus which formed at or near accretionary plate boundaries. We suggest that these volcanic ridges and the gross plateau like morphology were formed by magma that was channelled along the lithospheric discontinuities left behind by a southward propagating rift segment of the nearby spreading center. We attribute the formation of the northwestern portion of the Tuamotu Plateau to the passage of two hotspots during times 50-30 Ma as they migrated beneath the Pacific plate but remained west of the Tuamotu propagator.

Introduction

Hotspots in the mantle, are thought to be the sources of many crustal anomalies in the world's ocean basins. Oceanic hotspot features can be separated into two classes: island chains and oceanic plateaus. The morphological characteristics that distinguish these two classes may reflect differences in the tectonic environments at which they formed and/or the mantle sources which produced these melt anomalies. Ocean island chains are composed of discrete volcanic edifices with geographic age distributions reflecting the motion of the lithosphere with respect to the hotspot reference frame [*Duncan and McDougall,* 1976; *Clague and Jarrard,* 1973; *Morgan,* 1972]. As demonstrated by isotopic and paleontological ages that are less than magnetic ages of the underlying lithosphere [*Jarrard and Clague*, 1977; *Henderson,* 1985], most island chains were formed midplate, far from oceanic spreading centers. As a result, most island chains are compensated by mechanically competent lithosphere with effective elastic thicknesses (typically 10-25 km) that thicken with age, consistent with a conductive cooling model for the lithosphere [*Watts,* 1978; *Watts et al.*, 1980].

Oceanic plateaus, on the other hand, are defined by their broad elevated surfaces which, in many cases (e.g., Ontong Java, Shatsky Rise, and Manihiki), are nonlinear in plan view and lack the geographic age distributions so typical among island chains. Most oceanic plateaus are thought to have originated from hotspots sited near or at oceanic spreading centers or rifted continental margins because (1) edifice ages are close to those of the surrounding seafloor [*Detrick et al.*, 1977]; (2) subsidence histories of oceanic plateaus match closely those of the surrounding seafloor [*Detrick et al.*, 1977]; and (3) oceanic plateaus are compensated by Airy isostasy indicating they loaded thin elastic lithospheres found near ocean spreading centers

Paper number 95JB00071.
0148-0227/95/95JB-00071$05.00

[*Detrick and Watts*, 1979; *Kogan*, 1979; *Sandwell and MacKenzie*, 1989]. In addition, plateaus such as Manihiki [*Winterer et al.*, 1974] and Kerguelen [*Munschy and Schlich*, 1987] show faulted structures which may have resulted from extensional processes at an oceanic spreading center. The broad continuous extent of oceanic plateaus may result from efficient penetration of heat and magma through the weak lithosphere at oceanic spreading centers [*Vogt*, 1974; *Okal and Batiza*, 1987]. Volcanic volumes of oceanic plateaus, representing 5-25% of the world's total volcanic production for the past 150 m.y. [*Larson*, 1991], are typically much larger than the volumes of island chains and may be the products of massive flood basalt eruptions generated at the onset of mantle plume activity [*Morgan*, 1972, 1981; *Richards et al.*, 1989].

The Tuamotu Plateau, in the south central Pacific, is a volcanic feature with characteristics of both island chains and oceanic plateaus (Figure 1). From a regional perspective, the platform appears plateau like, with a broad elevated surface of width 80-200 km. A closer look, however, reveals discrete volcanic pinnacles, the largest of which are now reef-covered atolls. The platform is a linear feature trending from northwest to southeast similar to Pacific island chains such as the Hawaiian chain, the Cook-Austral chain, and the Society Islands. However, the eastern portion of Tuamotu Plateau may have been emplaced near the paleo-Pacific-Farallon spreading center, as suggested by the underlying weak lithosphere with effective elastic thickness of 2-6 km [*Okal and Cazenave*, 1985].

The nearly parallel alignment of the Line Islands-Tuamotu chain with the Hawaiian-Emperor chain led *Morgan* [1972] to hypothesize that the two were formed concurrently by two stationary hotspots. He suggested that the northwesternmost portion of Tuamotu platform marked the change in plate motion recorded by the bend in the Hawaiian-Emperor chain dated at 42-43 Ma [*Clague and Jarrard*, 1973]. Subsequent paleontologic and radiometric age constraints, however, indicate that the northernmost Tuamotu islands formed as late as 47-55 Ma [*Martini*, 1976; *Jackson and Schlanger*, 1976; *Schlanger et al.*, 1984], thus preceding the Hawaiian-Emperor bend by as much as 9 m.y. Several hotspots are suggested to have formed the Line Islands chain, based on the geochronologic studies of *Schlanger et al.* [1984] and *Winterer* [1976], while two hotspots are hypothesized to have formed the Tuamotu Islands from tectonic studies of *Okal and Cazenave* [1985]. Thus, the origin of the platform may be more complex than the single hotspot mechanism originally suggested by *Morgan* [1972].

In this paper we investigate the sedimentary and volcanic

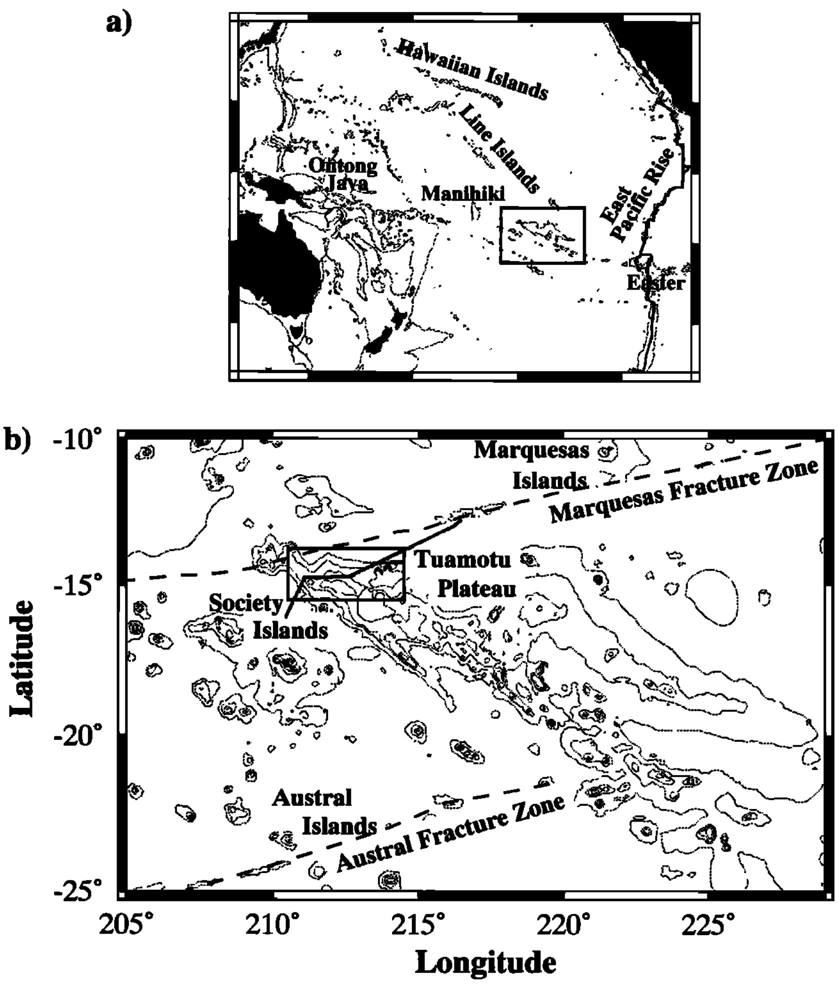

Figure 1. (a) Regional map surrounding the Tuamotu Plateau contouring the 3-km isobath. The rectangle outlines the bathymetry map below. (b) Bathymetry map of the Tuamotu platform with 1-km contour interval. The solid line marks the survey line which crosses the northern portion of the platform in the region marked by the rectangle.

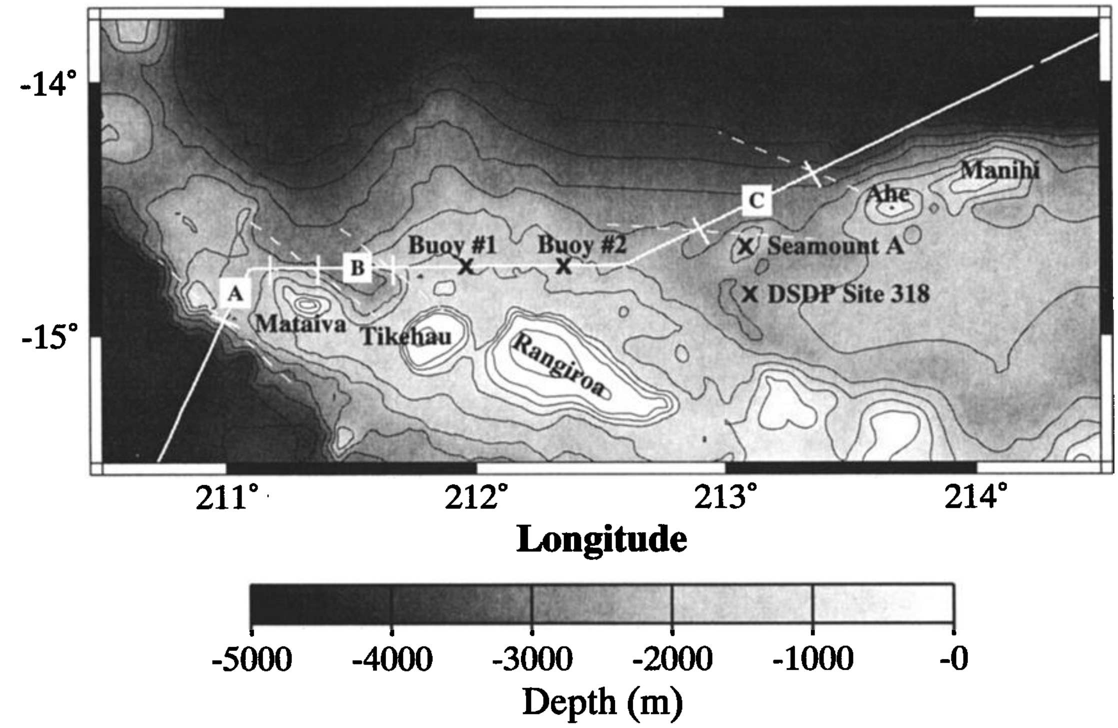

Figure 2. Bathymetry map of the survey region (rectangle in Figure 1b) with a contour interval of 500 m. The locations of the sonobuoy deployments are marked by X's along the survey track shown as solid white. Sections A, B, and C of the survey line are sediment basins revealed in the reflection profile. Dashed lines mark lineations of volcanic ridges and scarps inferred from the volcanic morphology observed in the reflection profile.

structure of the northwestern end of the Tuamotu Plateau in order to better understand the tectonic and magmatic processes controlling its formation. We image the shallow crustal structure (upper ~2 km) with multichannel seismic (MCS) reflection data obtained along a ship crossing of the northern portion of the platform. The velocity structure used for stacking the reflection data and for interpretation of sedimentary composition is derived from semblance analyses of the MCS data and from sonobuoy refraction data. To constrain the deep crustal structure and strength of the compensating lithosphere, we use gravity and bathymetry data. While the volume and flux of Tuamotu volcanism may have been controlled by the mantle source which was of comparable strength to the Hawaiian and Marquesas hotspots, the volcanic morphology of the Tuamotu platform may have been formed by structural discontinuities in the lithosphere, engraved by a propagating segment of the nearby Pacific-Farallon spreading center.

Data Collection

To reveal subsurface stratigraphy of the sedimentary and volcanic layers, we obtained multichannel reflection data along the survey line shown in Figures 1 and 2. We used the MCS system on board the R/V *Maurice Ewing,* which consisted of a 20-airgun (8385 in^3) array which shot to a 148-channel streamer with maximum channel offset of ~3.7 km. Shot spacing was ~50 m, yielding 37-fold, common-midpoint shot gathers; the sampling interval was 4 ms. The line was shot while steaming northeast to southwest. To constrain deep crustal velocities, we launched three expendable sonobuoys (buoys 1-3, Figure 2) which recorded refractions of the air-gun signal out to offsets of ~20 km.

Gravity data were collected with a KSS-30 gravimeter, while bathymetry was determined from the center beam readings of the Hydrosweep multibeam system. The bathymetry surrounding our ship track are digitized points from bathymetry maps produced at the Institut Francois de Rechere pour l'Exploitation de la Mer (IFREMER) and are from the Digital Bathymetric Data Base 5 (DBDB5) data set (Figure 2). Also shown in Figure 2 is the location of Deep Sea Drilling Project (DSDP) site 318, which penetrated 745 m into the sedimentary layer of the northern flank of the platform. Correlation of the drill core findings with our velocity results will be discussed below.

Seismic Reflection Data Analysis

Prestack Processing

Before stacking the MCS data, we performed three processing steps using the software package ProMax (ProMax 40.22, Advance Geophysical Corporation, copyright 1989-1992). In the first step, we applied a band-pass filter (5-62 Hz) to each channel record to eliminate low-frequency streamer noise and undesired high frequencies. The second step was to filter the shot gathers in frequency-wavenumber (*f-k*) space to eliminate energy which coincided with apparent velocities less than the water velocity (1.5 km/s), thereby reducing coherent noise seen as steeply dipping lines in unfiltered stacked data. Such coherent noise may have arisen from waves traveling from source to receiver through the streamer cable or guided in the water column, or by scattering from out-of-plane point sources [*Larner et al.,* 1983].

The final step in the prestack processing was predictive deconvolution. For each channel record, we specified two time gates from which we designed deconvolution filters. We set the

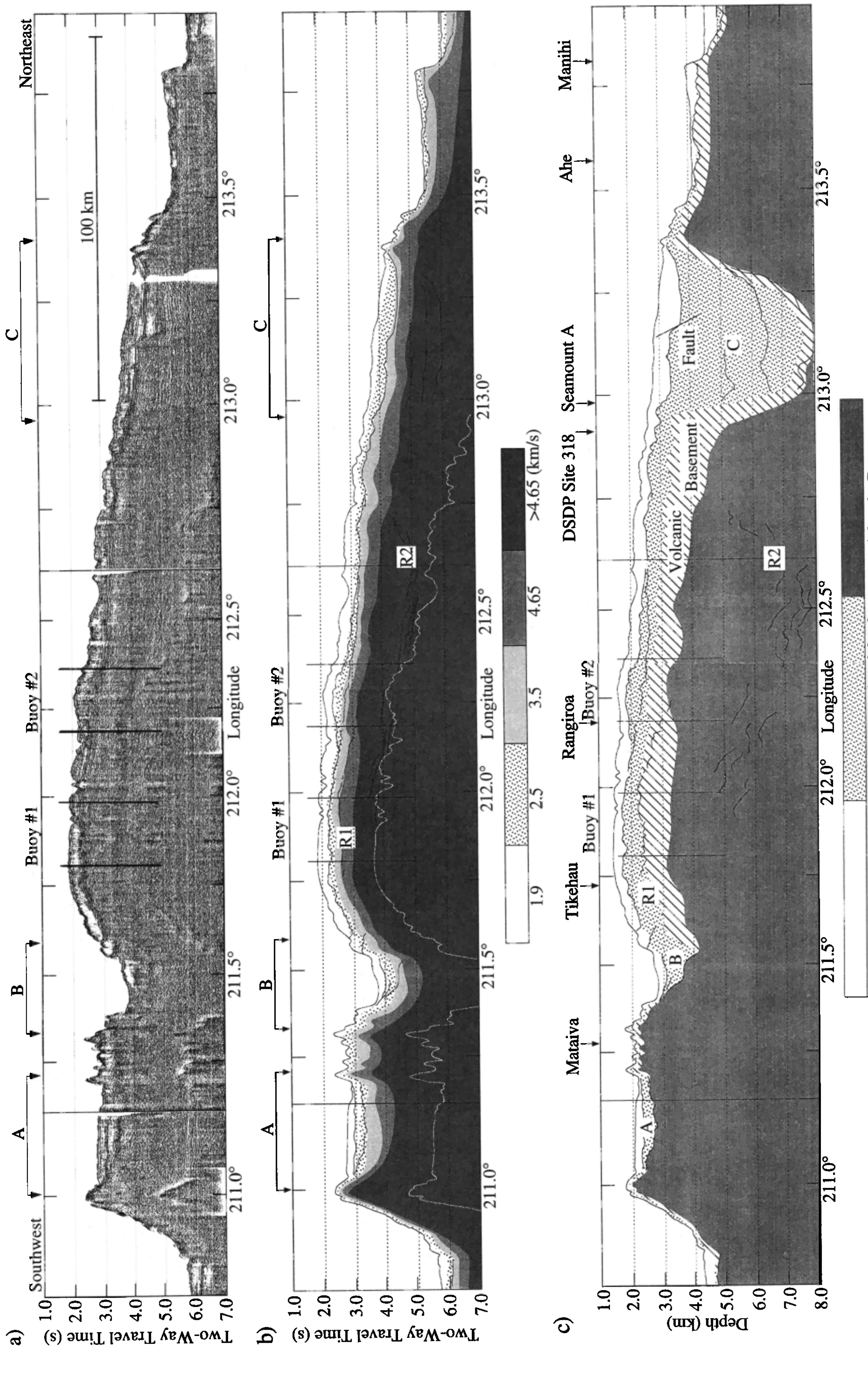
a)
Two-Way Travel Time (s)
1.0
2.0
3.0
4.0
5.0
6.0
7.0
Southwest
Northeast
A
B
C
Buoy #1
Buoy #2
100 km
211.0°
211.5°
212.0°
Longitude
212.5°
213.0°
213.5°
b)
Two-Way Travel Time (s)
R1
R2
1.9
2.5
3.5
4.65
>4.65 (km/s)
c)
Depth (km)
8.0
Mataiva
Tikehau
Rangiroa
DSDP Site 318
Seamount A
Ahe
Manihi
Volcanic
Basement
Fault
Pelagic Ooze, Chalk
Limestone, Volcaniclastics
Volcanic Crust

length of the upper gate to be between 0.5 and 1.5 s, so as to include the seafloor arrival and shallow sediment layers, and the length of the lower gate to be between 1.0 and 2.0 s, to include arrivals below the first gate but above the seafloor multiple. We applied the solution of the upper gate to data within and above the upper gate, and the solution of the lower gate within and below the lower gate. This two-gate procedure was chosen to account for changes in frequency character with increasing travel time, presumably due to both changes in sediment lithology and increased attenuation of the higher frequencies with depth.

A preliminary stacking without deconvolution produced a series of reverberations beneath many of the primary reflectors which, in the Fourier transform domain, showed as peaks at 13, 18, 25, 32, and 36 Hz. The direct water arrival signal had a similar amplitude spectrum, suggesting that many of the signals in the stacked section were artifacts of incomplete cancellation of the bubble-pulse signals from the airgun source array. Reverberations observed deeper in the stacked section might have also been generated by multiple reflections within subsurface sedimentary layers (i.e., peg-leg multiples). Our predictive deconvolution method proved effective in suppressing these undesired signals.

Results

After applying deconvolution, the data were sorted to common-midpoint gathers (CMP's), corrected for normal moveout using semblance-derived velocities, and then stacked. The stacked time section is shown in Figure 3a, while the reflections we identify are shown in Figure 3b. Between regions B and C (211.6°-212.9°E which we will refer to as the central portion) the plateau is draped by a layer of thickness 0.2-0.6 s (two-way travel time) characterized by rippled, but nearly continuous reflections (layer 1). The lower boundary of this layer is the horizon immediately below the seafloor marked in Figure 3b. Below this horizon is layer 2, characterized by slightly less continuous reflectors and more high-frequency noise between reflectors relative to layer 1. The lower boundary of layer 2 is defined by the deepest reflections in regions marked A, B, and C, but is uncertain within the central portion of the plateau. In the central portion of the plateau we observe reflections (R1, Figure 3b) that nearly parallel layer 1, 0.6-0.9 s below the seafloor. The deepest reflections we identify are a number of discontinuous reflections (R2), 1.6-2.5 s below the plateau surface. The crustal velocities shown in Figure 3b and the depth section shown in Figure 3c are discussed later.

Regions A, B, and C differ from the rest of the plateau in that reflections are nearly horizontal, smoother, and more continuous (Figure 4). Layer 1 is bound by the seafloor (reflector a) and reflector b, while layer 2 is bound by reflectors b and c. In region A, layers 1 and 2 are approximately the same thickness with combined thickness ~0.7 s. In region B, layer 1 is 0.2-0.4 s thick and overlies layer 2 which thickens eastward from 0.2 s to 0.9 s. In region C, the two layers extend as deep as ~2.3 s below the seafloor.

Region A and the east side of region C are bound by scarps of pinnacle like structures, the peaks of which are capped by very little sediment and reveal no reflectors below their opaque surfaces. The seismic records within these three regions resemble those of lagoonal sequences over the Mid-Pacific Mountains observed by *Winterer et al.* [1993], suggesting these stratigraphic sections are basins of carbonate sediments filled by continuous sediment influx from the surrounding volcanic slopes.

Velocity Analysis

Accurate constraints on crustal elastic wave velocities are important for high-quality stacking of the MCS data and for interpretation of sedimentary and crustal composition. Semblance calculations were made every 10 CMP's, then two to five adjacent calculations were stacked to enhance the signal to noise ratios. We used these stacked semblance results to pick root-mean-square (rms) velocities.

To constrain deeper crustal velocities, we used wide-angle refractions recorded by two sonobuoys over the central portion of the plateau in addition to the semblance analyses. Sonobuoy 1, launched near 211.9°E, recorded refractions out to an offset of ~22.0 km as the ship steamed west. Sonobuoy 2, deployed ~30 km east of sonobuoy 1, recorded refractions out to an offset of ~17.5 km. To determine crustal velocities, we performed forward modeling by one-dimensional (1-D) raytracing using the interactive raytracing feature of JDSeis (JDSeis, by John Diebold, Lamont Doherty Earth Observatory, Palisades, New York, 1992) and two-dimensional (2-D) raytracing using the software package MacRay [*Luetgert*, 1992]. Before the raytracing was done, however, sonobuoy records were corrected for topographic effects using the method described by *Officer and Wuenschel* [1951].

Figure 5 shows the sonobuoy records and raytracing curves with their corresponding velocity profiles. The direct water wave is seen as the linear arrival in the sonobuoy records. Arrivals a, in the sonobuoy records, are reflections from the base of the

Figure 3. (opposite) (a) The stacked time section of the Tuamotu Plateau shown from west to east which includes 25,780 CMP traces spanning ~360 km. For plotting, we stacked every four traces and applied a cubic polynomial gain function. The course changes shown in Figure 2 are marked by the bold vertical lines while the regions sampled by sonobuoys are marked by the short vertical lines. (b) Time section showing major reflections and semblance-derived interval velocities. The shallowest subsurface reflections correlate with the base of the lowest velocity layer (layer 1, white). The seafloor multiple is outlined in white. The central portion of the plateau (211.6°-212.9°E) is between regions B and C. (c) A depth section plot obtained from semblance velocities showing reflections and sediment compositions inferred from findings at DSDP site 318. The upper pelagic layer is white, while the lower limestone/volcaniclastic layer is dotted. The hachured region is the 4.65 km/s velocity layer which most likely encloses the volcanic basement interface in the central portion of the plateau. The shaded region marks the volcanic crust. Reflections R1 may be from the volcanic basement, while reflections R2 may mark a compositional volcanic boundary. Atolls, seamounts, and DSDP site 318 are marked at locations perpendicular to the ship track.

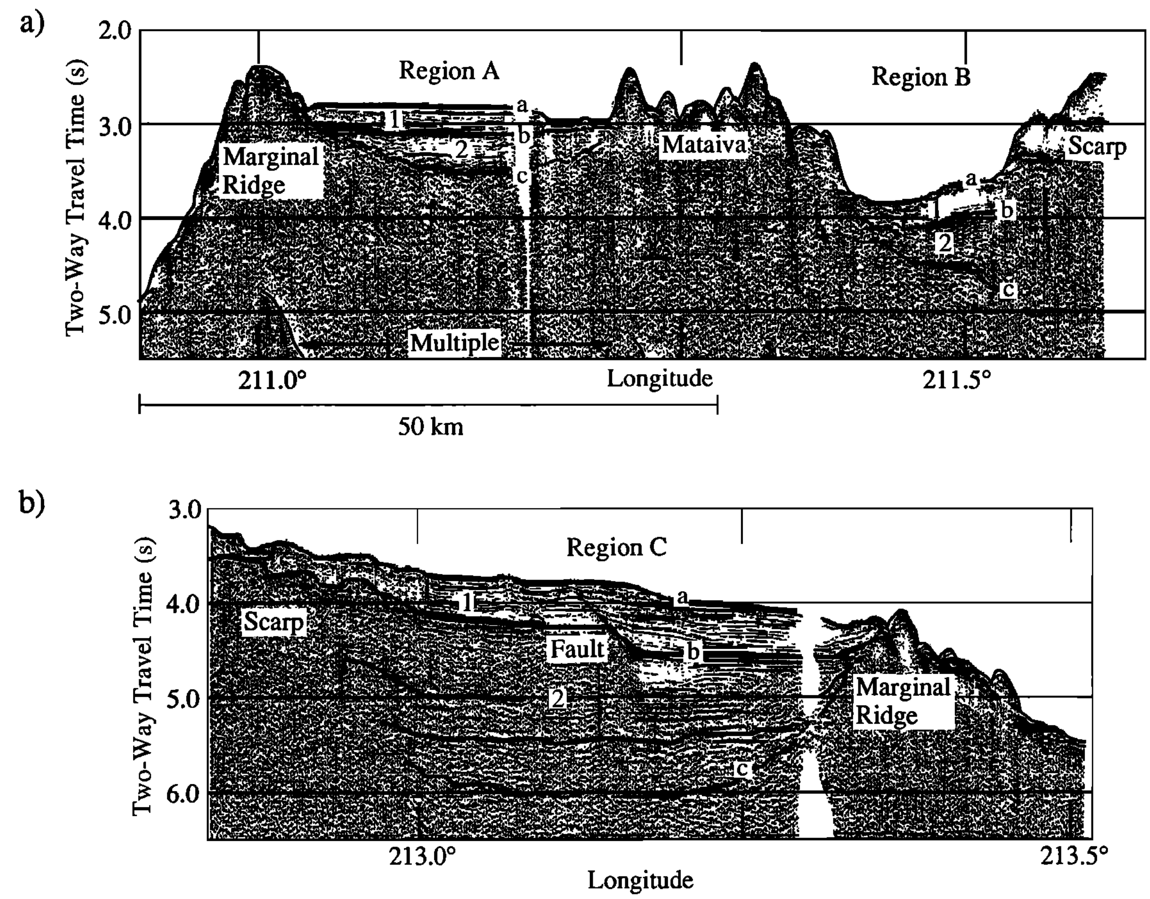

Figure 4. Reflection time sections marked along major reflectors designated by letters for (a) regions A and B and (b) region C. Reflection a is the seafloor, reflection b marks the base of layer 1 (the low velocity sediments), and reflection c marks the volcanic basement interface, also the lower bound of sediment layer 2. Bounding scarps and volcanic mounds are linear features seen in the survey map of Figure 2.

water column (velocity 1.5 km/s). Arrivals b, immediately below the seafloor arrival, are from the base of a low-velocity layer (1.6-2.0 km/s, layer 1) with approximate thicknesses of 0.35 km below sonobuoy 1 and 0.48 km below sonobuoy 2.

In the sonobuoy 1 record, deep refractions cross the seafloor arrival near an offset of 3.6 km. These refractions are from a high-velocity region in which we distinguish two layers: (1) layer 2, of thickness ~1.4 km and velocity 3.7-4.0 km/s, evident by first arrival refractions recorded out to an offset of ~10 km; and (2) layer 3, with thickness >1.8 km and velocities 4.3-5.0 km/s evident by first arrivals recorded at offsets >10 km. The combined thickness of the two layers is at least ~3.5 km. The high-velocity region sampled by sonobuoy 2 has a more continuous velocity profile which we identify as a single velocity layer (layer 2). Refracted energy from this layer first intersects the seafloor arrival, 2 km further in offset than in the sonobuoy 1 record, indicating a more gradual increase in velocity below layer 1. Layer 2 velocities increase to ~5.4 km/s over a thickness of ~3.4 km. The transition between layer 2 and layer 3 obtained by sonobuoy 1 may be the sediment-volcanic basement transition. This transition, however, is less evident in the sonobuoy 2 record because the sediments overlying the volcanic basement in this region have greater velocities, approaching those of basement, possibly due to higher volcaniclastic content.

For comparison, we also plot in Figure 5 the semblance-derived interval velocities at the midpoint depths of velocity layers for semblance calculations within the range of each sonobuoy record. The raytracing methods and semblance analyses produce consistent results for the first ~1.5 km (~1.0 s) below the seafloor; however, semblance velocities are slightly higher than raytracing velocities at depths greater than ~1.5 km beneath the seafloor. The consistency between semblance results and sonobuoy results in the upper 1 s strengthens our confidence in semblance-derived velocities above this depth.

We show semblance-derived velocity layers for the whole platform in Figure 3b. Layer 1 identified in the stacked section correlates well with the interval of velocity less than 1.9 km/s shown as the white layer immediately beneath the seafloor. Layer 2 is composed of two velocity layers: the first with average velocity 2.5 km/s and thickness 0.1-0.4 s, and the second with average velocity 3.5 km/s and thickness 0.1-0.5 s. An interval with average velocity of 4.65 km/s occurs 1.0-1.7 s below the seafloor. This interval is the last we chose to shade because its velocity is that at which the semblance-derived velocities began to deviate from sonobuoy-derived velocities. The velocity of 4.65 km/s is also the velocity that *Talandier and Okal* [1987] attribute to the extrusive basaltic layer from their regional refraction study. Depth uncertainties for the intervals range from 0.1 km for the 1.9-km/s velocity contour, to 0.5 km for the 4.65-km/s contour.

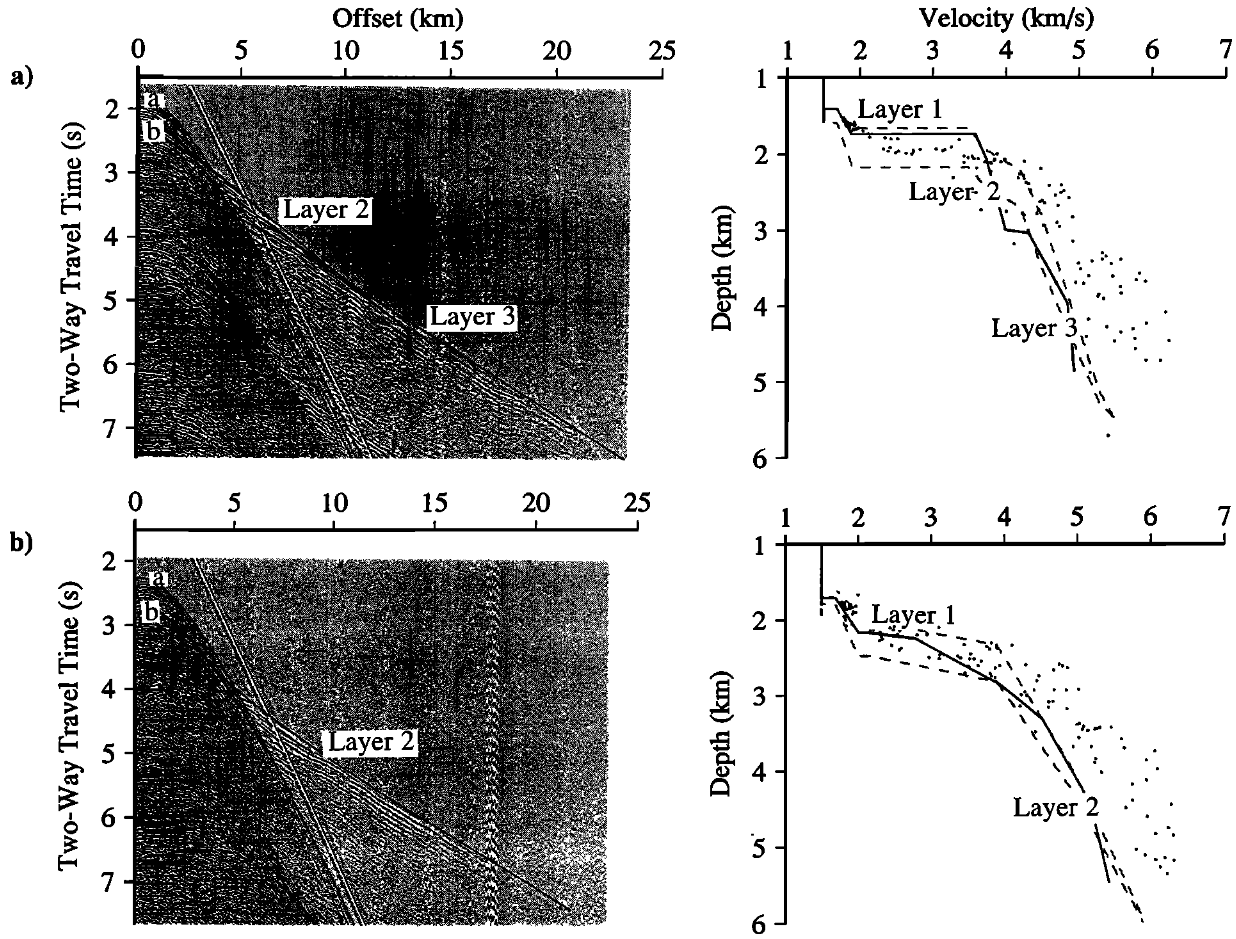

Figure 5. Sonobuoy records outlined with the 1-D raytracing curves, and corresponding velocity profiles for (a) sonobuoy 1 and (b) sonobuoy 2. The solid velocity profiles are the 1-D raytracing solutions which are consistent with the shallowest and deepest velocity nodes of the 2-D raytracing solutions connected by the dashed lines. The dots mark interval velocities at the midpoint depths of each velocity layer for semblance calculations within the range of the sonobuoy records. Semblance velocities begin to deviate from raytracing solutions at ~1.5 km below the seafloor and near a velocity of ~4.5 km/s. Arrivals a are the seafloor reflections and arrivals b, just below arrivals 1, are the base of the low-velocity sediment layers.

Sediment Composition and Volcanic Morphology

From these constraints on crustal velocities and from stratigraphy imaged by the stacked MCS data, we infer composition of sediments and structure of the underlying volcanics. We base our interpretations of sediment composition on the findings of DSDP site 318 which penetrated 745 m below the seafloor, ~25 km southeast of our survey line near 213°E [*Schlanger et al.*, 1976] (marked in Figure 3c and in the map in Figure 2). The compositions of the drill core sections are outlined in Table 1. The velocities of layer 1 correspond well with those for units 1 and 2 of the drill core; therefore, we interpret this upper layer to be pelagic ooze becoming more lithified with depth to form chalk. This is shown as the white layer in Figure 3c draping the central portion of the plateau (211.6°-212.9°E) with thickness 0.2-0.9 km. The velocities of layer 2 (2.5-3.5 km/s) correlate well with those for the lower two units of the drill core; therefore, we believe this layer is composed of chalk near the top, and limestone with increasing concentrations of volcaniclastic sediments near the bottom. This compositional layer is shown over the central portion of the plateau as the dotted layer in Figure 3c with thickness ~0.5 km. The compositional difference between layer 1 and 2 may explain the previously noted difference in reflection character between the two layers.

Within the layer of interval velocity 4.65 km/s lies the sediment-volcanic basement transition (with the exception of region C to be discussed below) shown as the hachured region in Figure 3c. Through most the central portion of the plateau, the volcanic basement interface is not evident in the reflection section presumably because of the small (or nonexistent) impedance contrast between the deep sedimentary rocks and surface extrusives. Reflections R1 (Figure 3), however, might be from this interface. The inferred volcanic basement between 211.75°E and 213.0°E gradually deepens from west to east with very little apparent relief. The total sediment thickness in this region is 1-2 km and suggests an average sedimentation rate of 20-40 m/m.y., assuming a basement age of 50 m.y. The bulk of this layer may have been built as reefs when the central portion of the plateau was near sea level. Then, as the platform subsided, the reefs drowned and were blanketed by pelagic sediments and sediments eroded from higher-standing edifices.

Table 1. Recovery From DSDP Site 318

Unit	Depth Range, m	Composition	Compressional Sound Velocity, km/s	Age
1	0.0-265.5	foram-nannofossil ooze grading to soft chalk, volcanic sand	1.6-2.0	Pleistocene
2	265.5-416.0	breccia and conglomerate basalt clasts, foram-nannofossil chalk, volcanic sand, and chert	1.7-2.0	lower Oligocene-upper Pliocene
3	416.0-530.0	foram-nannofossil limestone rich in reefal forams; corals, volcanic siltstone and sandstone	2.0-3.5	upper Eocene
4	530.0-745.0	nannofossil limestone, siliceous volcanic sandstone and siltstone	2.0-4.4	lower Eocene-middle Eocene

Geological data are from *Schlanger et al.* [1976], ages are from *Martini* [1976], and seismic velocities are from *Boyce* [1976]

Near stratigraphic regions A, B, and C, however, the volcanics form steep-sided mounds with little sediment covering over the peaks. The sediment basin in region A is bounded on the west by a volcanic ridge forming the western margin of the plateau and to the east by the slope of Mataiva atoll (see Figures 2 and 3). The volcanic basement forms a valley which has accumulated a sediment layer of thickness ~0.7 km. Again, assuming an age of 50 m.y. for the underlying volcanics, the average sedimentation rate for basin A is ~14 m/m.y. The sediment basin in region B is bounded on the west by a scarp extending from Mataiva and to the east by a nearly parallel scarp extending northwest from Tikehau. The total sediment accumulation for this basin is ~1.6 km, suggesting an average sedimentation rate of ~32 m/m.y. The sedimentation rates for these basins and for the central portion of the plateau are comparable with those at DSDP site 318 which range from 44 m/m.y., during the lower Pleiocene, to 6 m/m.y. during the lower Miocene.

The sediment basin in region C is bounded on the west by a scarp along the north side of a small seamount (seamount A, Figure 2). Volcanic basement in region C may lie as deep as 5.0 km below the present-day seafloor, corresponding to the predicted depth of the deflected, preexisting seafloor upon which the plateau formed (from lithospheric flexural models constrained by the gravity data as discussed later). Thus, the base of this deep valley may have never been covered by Tuamotu volcanism. The average sedimentation rate in region C is as much as ~100 m/m.y., several times that of the rest of the platform. Offsets in sediment stratigraphy through layer 1 and in the upper section of layer 2 indicate faulting, most likely from slumping of the sedimentary layer down the slope of seamount A. The more subdued topography near the northeastern margin compared with that of the southwestern margin may indicate that gravity slumping was more prevalent in the northeast. This might explain the much higher sedimentation rate for basin C relative to the rest of the platform.

The deep reflections, marked R2 (Figures 3b and 3c) begin at a depth of ~4.7 km near 212°E and deepen to almost 8.0 km near 212.5°E, where they reach ~6 km below the plateau's surface. These reflections are from a deep crustal impedance contrast, possibly the upper surface of the gabbroic layer underlying the basalts as suggested by *Talandier and Okal* [1987]. Talandier and Okal find a velocity of 6.83 km/s for this deep layer, which is consistent with our requirement that velocities exceed the 5.5-km/s maximum observed in the sonobuoy records to produce an impedance contrast sufficient to yield reflections. We further investigate the deep crustal structure from analysis of gravity data.

Compensation Mechanisms and Deep Crustal Structure

Determining the compensation mechanism of the Tuamotu Plateau is important in constraining the elastic strength of the lithosphere, which reflects the age of the underlying plate at the time of accretion. The compensation mechanism also is important in determining the volcanic thickness of the plateau and thus constraining the volume and flux of eruption, which reflect the nature of the mantle source. The interface between the base of the crust and mantle (Moho) was imaged with reflection data only outside of the plateau margins, restricting constraints on the depth and shape of the Moho to the sides of the plateau. Therefore, to constrain the deep crustal structure beneath the platform, we focus on the gravity and bathymetry which are both sensitive to variations in crustal thickness.

Crustal Compensation

Here we assume that the Tuamotu magmas loaded the upper surface of the preexisting seafloor, thereby downwarping the lithospheric plate. Thus, topography of the plateau is isostatically supported by the thickened crust, and the free-air gravity is the combined attraction of the seafloor-water interface and the Moho. Given the observed topography, we make predictions as to the shape of the Moho for different elastic-plate thicknesses (T_e). We then produce theoretical gravity profiles that we compare with the observed free-air gravity data. Since the gravity signal is sensitive to three-dimensional density structure, we perform the flexure and gravity calculations using the gridded bathymetry map but compare only those values coinciding with our ship track to the observed gravity.

A standard method of solving the 2-D, fourth-order, differential equation describing the deflection of an elastic plate loaded from above, is to solve the equation in the spectral domain. The solution of the 2-D transform of downward plate deflection W depends on the 2-D transform of topography H, according to

$$W = \frac{\Delta\rho_c}{\Delta\rho_m}\left[1 + \frac{(2\pi k)^4 D}{(\Delta\rho_m) g}\right]^{-1} H, \qquad (1)$$

in which $\Delta\rho_c$ and $\Delta\rho_m$ are the crust-water and mantle-crust density contrasts respectively, k is the amplitude of the 2-D wavenumber, and g is the acceleration of gravity. The flexural rigidity D depends on elastic plate thickness T_e, according to

$$D = \frac{E T_e^3}{12(1-\nu^2)}, \qquad (2)$$

where E is Young's modulus ($8\mathrm{x}10^{10}$ N/m^2) and ν is Poisson's ratio (0.25). Using *Parker's* [1973] spectral method, we calculate the combined gravity fields due to the 2-D topography and the deflection of the Moho. We then produced theoretical free-air gravity grids from which we extracted values coinciding with our ship track. The density of the water and mantle are assumed to be

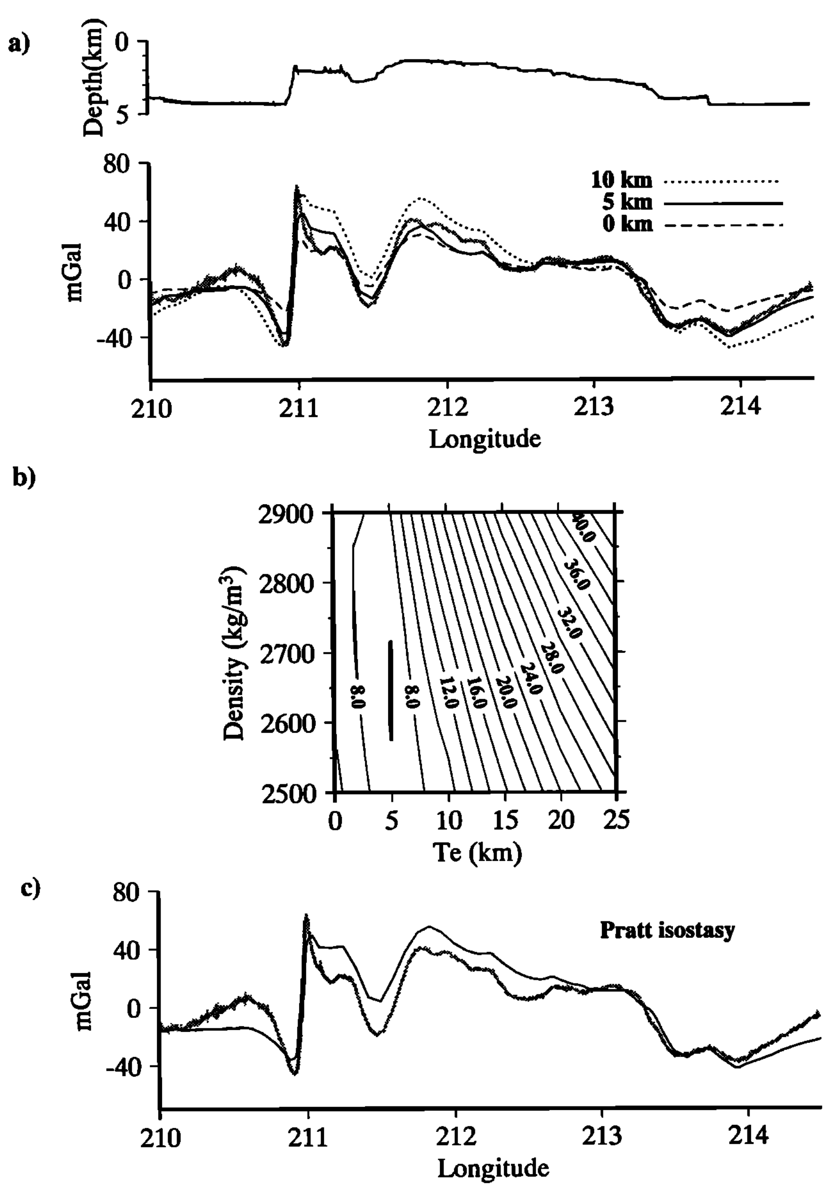

Figure 6. (a) The depth profile along the ship track lies above the observed free-air gravity profile (thick, gray-shaded) and theoretical profiles assuming an average crustal density of 2650 kg/m^3 and elastic plate thicknesses (T_e) of 0, 5, and 10 km. The elastic plate model for T_e=5 km yields the smallest standard deviation misfit of 5.9 mGal, while the models for T_e=0 and 10 km yield misfits of 9.7 and 11.9 mGal respectively. (b) Standard deviation misfits contoured at 2-mGal intervals for gravity models of crustal densities, 2500-2900 kg/m^3 and elastic plate thicknesses 0-25 km. (c) The observed and theoretical gravity profile assuming Pratt isostasy with a depth of compensation, z_c, of 20 km. The theoretical gravity includes the attraction due to the seafloor-water density interface; a crust-mantle interface assuming the crust is a constant 6 km in thickness and 2560 kg/m^3 in density; and lateral density variations in the mantle, $\Delta\rho$, set according Pratt's equation: $\Delta\rho=\rho_o H/z_c$, where ρ_o is the mantle-water density contrast (2300 kg/m^3) and H is topography.

1000 and 3300 kg/m^3 respectively and the two parameters we vary are T_e and $\Delta\rho_c$.

Theoretical profiles for elastic plate thicknesses 0, 5, and 10 km, and crustal density 2650 kg/m^3 are compared with observed free-air gravity profiles in Figure 6a. The 5-km-thick elastic plate model yields the lowest standard deviation misfit (5.9 mGal) to the data for this crustal density. Standard deviation misfits for elastic plate thicknesses ranging 0-25 km and for average crustal densities 2500-2900 kg/m^3 are contoured in Figure 6b. For all densities, misfits increase dramatically away from T_e= 5 km. The maximum of 44.0 mGal is obtained for T_e=25 km and crustal density 2900 kg/m^3. The lowest misfits (<6.0 mGal) are found for densities 2550-2750 kg/m^3 and T_e=5 km. Since all crustal densities examined yield minimum misfits near T_e=5 km, we conclude that the effective elastic plate thickness beneath the northwestern portion of the Tuamotu platform is 5±5 km. This thickness is similar to elastic plate thicknesses beneath the southern end of the plateau of 2-6 km, obtained from the geoid analysis of *Okal and Cazenave* [1985]. Our lowest standard deviation misfits (of which 1-2 mGal are the intrinsic error of the gravimeter) are higher than the 2-5 mGal misfits obtained by *Filmer et al.* [1993] over the Marquesas and Society Islands using the same technique, most likely due to the unmodeled 1 to 2-km-thick sediment layer present over Tuamotu volcanics but absent over the Marquesas and Society volcanics.

Pratt Compensation

While crustal compensation is clearly important, another source that may contribute to the compensation of the Tuamotu Plateau is lateral density variation in the lithosphere (Pratt-type isostasy) that may have resulted from varying degrees of partial melting of the mantle during the plateau's accretion. *Angevine and Turcotte* [1980] suggested that this compensation mechanism contributes significantly to supporting the topography of the Walvis Ridge in the South Atlantic. The theoretical gravity profile in Figure 6c is that predicted by assuming the topography of the plateau is compensated by lateral density variations in the mantle, 20 km below a crust with a uniform thickness of 6 km. The profile overestimates the amplitude of the observed gravity anomaly over the central portion of the plateau and underestimates the amplitudes to the sides of the platform which come from the flexed Moho. The standard-deviation misfit for this profile is 12 mGal becoming larger with increasing assumed depths of compensation. Thus our gravity modeling shows that the dominant source of compensation is low-density material within or near the base of the crust.

Deep Crustal Structure and Volcanic Production

As noted above, Moho reflections were observed in the MCS data to the sides of the plateau beneath the normal oceanic crust (Figure 7). These arrivals, while low in amplitude, are prevalent throughout these sections, consistently ~2 s below the volcanic basement which is blanketed by 0.2-0.5 s of pelagic sediments. Using a velocity of 6 km/s for the volcanic crust as constrained from the semblance data and refraction data from sonobuoy 3 launched near 214°E (see Figure 2), we constrain the local thickness of the oceanic crust to be 6±1 km.

By incorporating these constraints for the crust to the sides of the plateau with the deep crustal structure from the gravity modeling and the sedimentary structure over the platform, we summarize our crustal model in Figure 8. The shape of the Moho as derived from our best fitting flexural model (T_e=5 km and crustal density 2650 kg/m^3, solid curve) is consistent with the seismic observations to the sides of the Tuamotu platform. We show the top of the preexisting seafloor (dashed) assuming that all Tuamotu volcanism was emplaced on top of the 6-km-thick

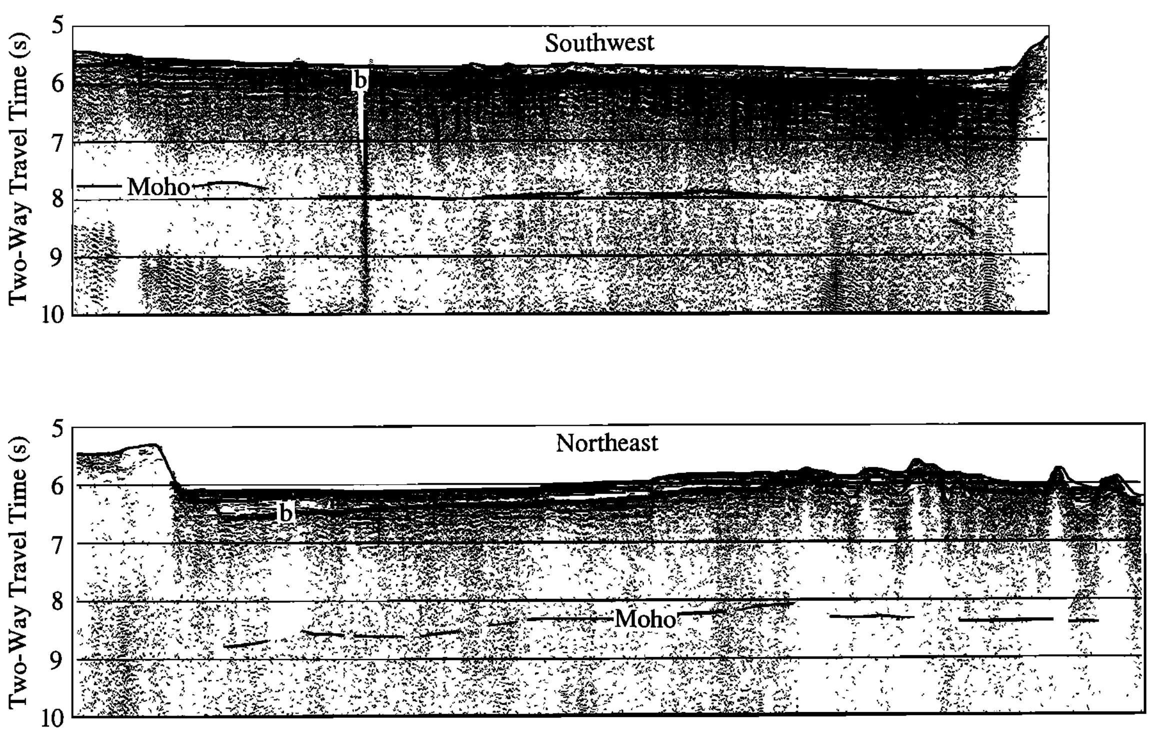

Figure 7. Time sections of the abyssal seafloor to the southwest and northeast of the Tuamotu Plateau. Moho arrivals are observed consistently ~2 s below the sediment-volcanic basement interface (marked b).

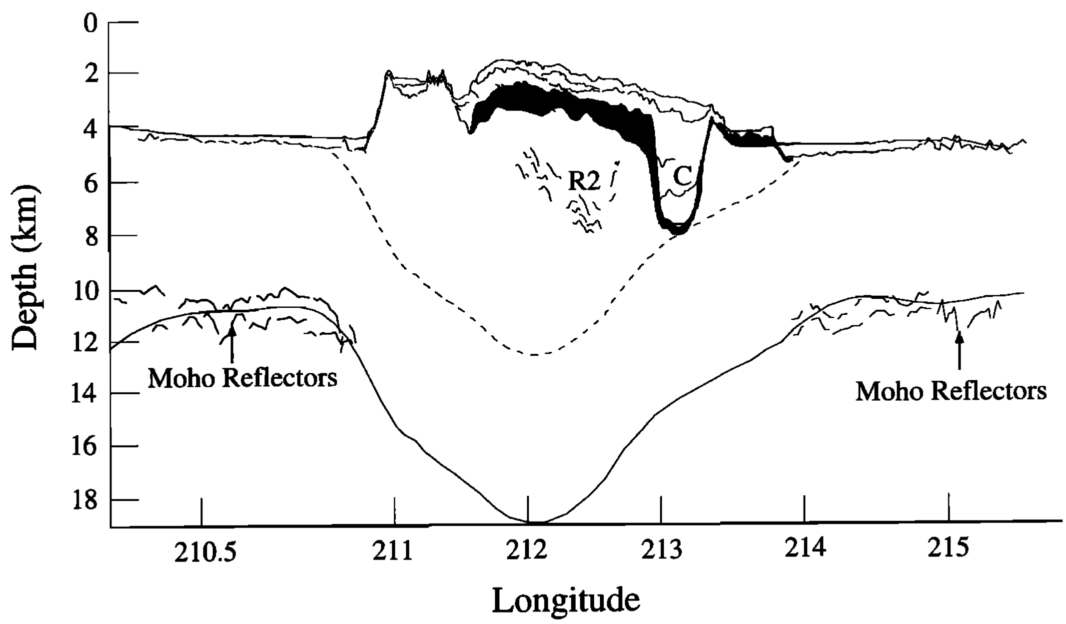

Figure 8. Depth profile along the ship track showing sedimentary layer 1, the estimated location of the volcanic basement (shaded), Moho reflections in the surrounding seafloor, and the theoretical Moho profile of our best fitting elastic plate model (solid). The dashed line marks the preexisting seafloor assuming the Tuamotu platform loaded the upper surface of a uniform, 6-km-thick oceanic crust.

oceanic crust. Note that the base of region C, lies near the preexisting seafloor, indicating as mentioned previously, that there may have been very little excess volcanism in this basin. The R2 reflections lie 3-9 km above the preexisting seafloor, midway between the preexisting seafloor and sediment-basement interface. We conclude that the maximum crustal thickness along our profile is ~18 km, the maximum total volcanic thickness is 16-17 km, and the maximum excess volcanic thickness (i.e., in addition to a 6-km-thick normal oceanic crust) is 9-10 km.

From these constraints we can estimate the total volcanic production of the Tuamotu hotspot. Using the gridded bathymetry map of the region, we sum the volume from the topography (ie., shallower than the average depth of the surrounding seafloor 4.2 km), as well as the volume of the compensating crustal root, assuming the entire platform is compensated by an elastic plate thickness of 5 km. From this volume we subtract the sediment volume, assuming a sediment thickness of 0.2-0.3 km beneath seafloor deeper than 3.5 km and 1-2 km beneath seafloor shallower than 3.5 km. Our estimate for the total volcanic volume of the plateau is 7.3-7.8x10^6 km^3 and our estimate for the excess volcanic volume (ie., subtracting the volume of a 6-km-thick layer) is 2.0-2.6x10^6 km^3. If we assume a fixed hotspot, the Pacific plate took 20 m.y. to migrate along the length of the platform (from absolute Pacific plate rotation rates of *Duncan and Clague* [1985]). This time span for the plateau's formation yields average volcanic fluxes, including and excluding 6 km of the crust, of ~0.4 and 0.1 km^3/yr respectively. The volume and fluxes which include 6 km of the crust may be the most appropriate estimates if the plateau formed on-axis, while those which exclude the normal oceanic crust may be the most appropriate, if the plateau formed off-axis.

To characterize the mantle source which gave rise to the Tuamotu Plateau, we compare volcanic volumes for the platform with those of two island chains and five oceanic plateaus in Figure 9a. The volumes of the five plateaus include the surface and subsurface volumes assuming topography is compensated by Airy isostasy [*Schubert and Sandwell*, 1989]. The volume estimate for Hawaii, considers only the volume of surface topography of the chain from the Emperor Seamounts to the island of Hawaii (it does not include the compensating crustal root, but this may be offset by the fact that it does include the topographic swell not associate with crustal thickening). The volume estimate for the Marquesas Islands from *Wolfe et al.* [1994] includes the volumes from the topography and compensating roots as well as the volume of the volcanic sediments filling the surrounding flexural moat as constrained seismically. The excess volcanic volume of the Tuamotu platform is significantly larger than the volume of the Marquesas Islands; and although the Tuamotu Plateau is morphologically distinct from Hawaii, the excess Tuamotu volume is comparable to that of Hawaii. The Tuamotu Plateau is significantly smaller than the other plateaus despite its morphological similarity.

Possibly, more telling as to the nature of the mantle source of these volcanic features is the rate at which these volumes were extruded (Figure 9b). We derive the volcanic fluxes for Manihiki and Ontong Java Plateaus (1.7-4.4 and 7.9-16.9 km^3/yr respectively) by dividing the volumes by the 3-m.y. duration of volcanism as estimated from drill core findings [*Tarduno et al.*, 1991; *Coffin and Eldholm*, 1993], and flux rates for Broken Ridge and Kerguelen (1.2-2.8 and 5.5-9.9 km^3/yr respectively) by dividing by the volcanic duration of 4.5 m.y. also from drill core data [*Coffin and Eldholm*, 1993]. Volcanism along the Walvis Ridge, between the continental margin of Africa and ~36°S, ensued for ~70 m.y. according radiometric dating results of *O'Connor and Duncan* [1990] which yields an average eruption rate of 0.1-0.2 km^3/yr. Eruption fluxes for Hawaii and the Marquesas Islands (0.5 and 0.4 km^3/yr respectively) as estimated by *Filmer et al.* [1994], are the average fluxes over the past 6 m.y.; they include topographic and compensating volumes as well as the volumes of the sediment-filled moats. The flux estimates

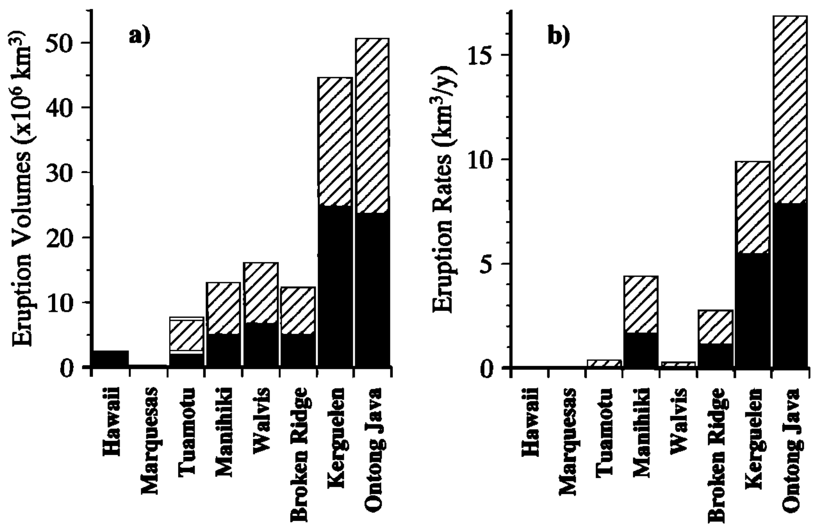

Figure 9. Bar graphs of the estimated (a) eruption volumes and (b) eruption rates of the Hawaiian and Marquesas Island chains, the Tuamotu Plateau, and five oceanic plateaus. White hachured bars denote estimations using the total volcanic volumes; black bars denote values using only the excess volcanic volumes (i.e., total volume minus the volume of the normal oceanic crust: 6 km in thickness as constrained in this study for the Tuamotu Plateau, and 6.5 km in thickness as used by *Shubert and Sandwell* [1989] for the other edifices). The uncertainty range for the Tuamotu total and excess volumes are the unpatterned sections of the bar.

for the Tuamotu Plateau are most comparable with those of Hawaii and Marquesas and, with the exception of the Walvis Ridge, substantially less than the other oceanic plateaus. Again, the mantle source which generated Tuamotu magma is similar in both size and longevity to the hotspots which have formed Hawaii and the Marquesas. The Walvis Ridge source, although liberating a greater magmatic volume, appears to be a long lived hotspot similar to the Tuamotu hotspot. The other oceanic plateaus appear to have formed by a very different phenomena which involved dramatic flood-basalt volcanism.

Implications for the Origin of the Tuamotu Plateau

Proximity to the Pacific-Farallon Spreading Center

If the mantle source of Tuamotu volcanism is a hotspot much like the Hawaiian and Marquesas hotspots, we must now explain why the continuous volcanic ridges and plateau like form of the Tuamotu Plateau differ from the discrete pinnacles that compose the two island chains. To better understand the magmatic and tectonic processes which constructed the northwestern end of the Tuamotu Plateau, we must first consider the tectonic setting in which the plateau formed. The proximity of the Tuamotu Plateau to the Pacific-Farallon paleo-spreading center (at which the underlying oceanic lithosphere was created) can be inferred from available age constraints for the plateau compared with geomagnetic ages of the surrounding seafloor. The minimum age of the northwestern end of the platform is constrained by the age of the oldest sediments sampled on the plateau (Figure 10): lower middle Eocene, from a dredge haul along the southwestern margin near 14.5°S [*Burckle and Saito,* 1966]; lower Eocene, from DSDP site 318 [*Martini,* 1976]; and middle Eocene, from dredge hauls along the southwestern margin near 16.5°S [*Le Suave et al.,* 1989]. Volcanic samples from the plateau are from two dredge hauls along the southwestern margin very near our survey line with ^{40}Ar-^{39}Ar dates of 41.8±0.9 Ma and 47.4±0.9 Ma [*Schlanger et al.,* 1984]. Thus, accretion of the northern portion of the Tuamotu Plateau may have begun as early as 55 Ma and persisted to at least 41.8 Ma.

When considering the results of a recent magnetic study by *Antoine et al.* [1993], the above ages suggest that the northern portion of the Tuamotu platform formed significantly off the axis of the Pacific-Farallon spreading center. As illustrated in Figure 10, the section of the plateau near our survey line is underlain by oceanic crust with ages ~64-71 m.y.; therefore, an age of 50-55 m.y. for the northern plateau suggests that it was emplaced on lithosphere of age ~10-20 m.y. The spreading center at this time was approximately 600 km to the east of the plateau (Figure 10). A lithospheric plate with age 10-20 m.y. would have an effective elastic thickness of 10-15 km, assuming T_e corresponds to the depth of the 450°C lithospheric isotherm [*Watts,* 1978; *Watts et al.,* 1980]. This range of thickness is slightly greater than our upper bound of 10 km obtained from our gravity modeling possibly because the regional lithosphere may be anomalously warm [*McNutt and Fischer,* 1987], thus yielding extremely small values of T_e [*Menard and McNutt,* 1982; *Calmant and Cazenave,* 1987]. Errors in the geomagnetic timescale of *Berggren et al.* [1985] are likely to be less than 2-3 m.y. (see Figure 30 of *Cande and Kent* [1992]); therefore, unless the age constraints for Tuamotu volcanism are significantly in error, it is unlikely that the northwestern end of the Tuamotu Plateau formed at the Pacific-Farallon paleo-ridge.

The inferred subsidence of the plateau is also consistent with the 10-20-m.y. age difference between the plateau and the underlying lithosphere. Isostatic removal of the 1-2 km-thick sediment layer (using an average sediment density of 2100 kg/m^3 [*Schlanger et al.,* 1976]) would put the basement depth over the central portion of the plateau at 1.6-2.1 km. This depth range may reflect the subsidence of the plateau if it was once near sea level, as suggested by the reefal sediments obtained at DSDP site 318. Such a range of subsidence is expected if the plateau loaded a cooling lithospheric half-space of age 5-14 m.y., consistent with

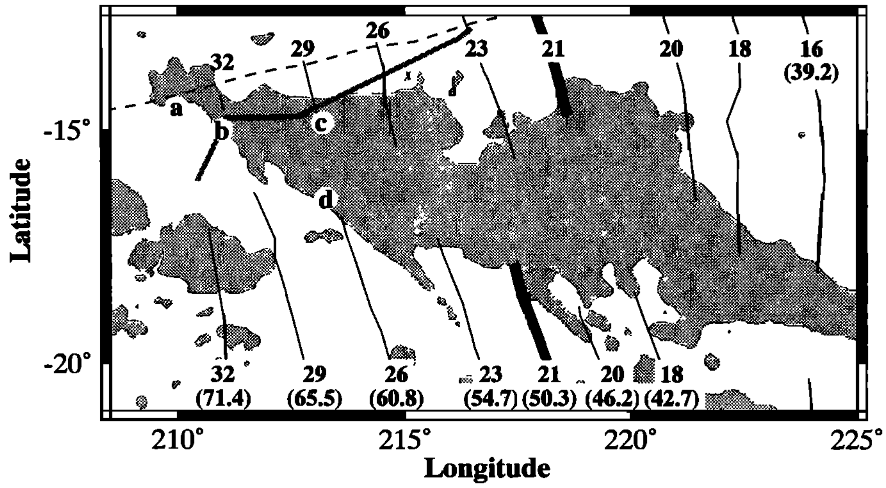

a- Lower Middle Eocene (44-51 Ma) [Burckle and Saito, 1966]
b- 40.9-48.3 Ma [Schlanger et al., 1984]
c- Lower Eocene (52-55 Ma) [Martini, 1976]
d- Middle Eocene (40-51 Ma) [Le Suave et al., 1989]

Figure 10. Map of magnetic lineation anomalies [*Antoine et al.*, 1993] surrounding the Tuamotu Plateau (shaded for depths <3500 m) marked with anomaly numbers and corresponding ages (Ma) [*Berggren et al.*, 1985]. The configuration of the paleo-spreading center near the time of formation of the plateau is shown by the thickest isochron labeled with its age, 50.3 m.y. Locations of sediment and crustal samples are labeled according to their ages and sources as listed. Our ship track is marked by the thick line crossing the northwestern end of the platform.

our age estimate of 10-20 m.y. The predicted subsidence, assuming a plate age of 10-20 m.y. at the time of loading, is 1.8-1.4 km, much less than the ~3 km of subsidence predicted if the plateau formed on axis.

Morphological Similarities: The Manihiki Plateau and the Walvis Ridge

Although the ages for the platform and underlying seafloor indicate an off-axis origin for the Tuamotu platform, the volcanic morphology is similar to that of many oceanic plateaus that formed at oceanic spreading centers. When considered with the surrounding bathymetry, the volcanic scarps and mounds imaged by the reflection seismics appear to be linear features with roughly northwest to southeast lineaments (Figure 2). Despite the numerous seamounts and atolls scattered throughout the Tuamotu platform, the dominant crustal fabric appears to be continuous, elongated volcanic features quite unlike what is found within midplate island chains.

Two oceanic plateaus with ridges and scarps similar to the Tuamotu platform are the Manihiki Plateau, located ~1000 km northwest of the Tuamotu Plateau (Figure 1a), and the Walvis Ridge which extends southwest from the continental margin of Africa into the southern Atlantic. The basement rim along the eastern margin of the Manihiki Plateau [*Winterer et al.*, 1974] bears close resemblance, in both shape and scale, to the southwestern marginal ridge of the Tuamotu platform (Figure 11a). The Manihiki marginal ridge stands ~3.4 km above the seafloor of the Penrhyn Basin and, like the Tuamotu margin, forms a barrier bounding the plateau sediments. Ridges and faults observed in seismic profiles along the eastern margin of Manihiki Plateau led *Winterer et al.* [1974] to hypothesis that this margin formed either along a paleo-transform fault separating the Farallon and Antarctic plates, or along the paleo-spreading axis separating the Antarctic and Pacific plates. A recent magnetic and gravity survey to the east of the plateau by *Munch et al.* [1992] supports *Winterer et al.*'s later hypothesis.

The Walvis Ridge is also similar to the Tuamotu Plateau in many aspects. It is bordered to the north by a volcanic ridge and is composed of numerous volcanic ridges. The profile in Figure 11b, obtained from the seismic profile of *Goslin and Sibuet* [1975], illustrates the northern margin of the Walvis Ridge, which stands >2 km above the seafloor and dams the plateau sediments. The Walvis Ridge is also similar to the Tuamotu platform in the asymmetry of their corresponding profiles: the abrupt northern margin and gradual tapering of the southern margin of the Walvis Ridge resembles the southwestern and northeastern margins of the Tuamotu Plateau, respectively. *Goslin and Sibuet* [1975] suggest that the Walvis Ridge formed during or near the initial breakup of the African and South American continents, and that the northern Walvis margin marks the boundary of a paleo-transform fault.

Model for the Formation of the Tuamotu Platform

Thus, when considering the Manihiki Plateau and Walvis Ridge examples, it is likely that the formation of the linear volcanic features of the Tuamotu Plateau was influenced by tectonic structures in the underlying crust and lithosphere. Structures related to rifting at an ocean spreading center as in the case of the Manihiki Plateau can be excluded, since the Tuamotu platform was formed significantly off-axis and the plateau lineaments are oblique to seafloor isochrons. Likewise, it is unlikely that the Tuamotu platform formed along a transform

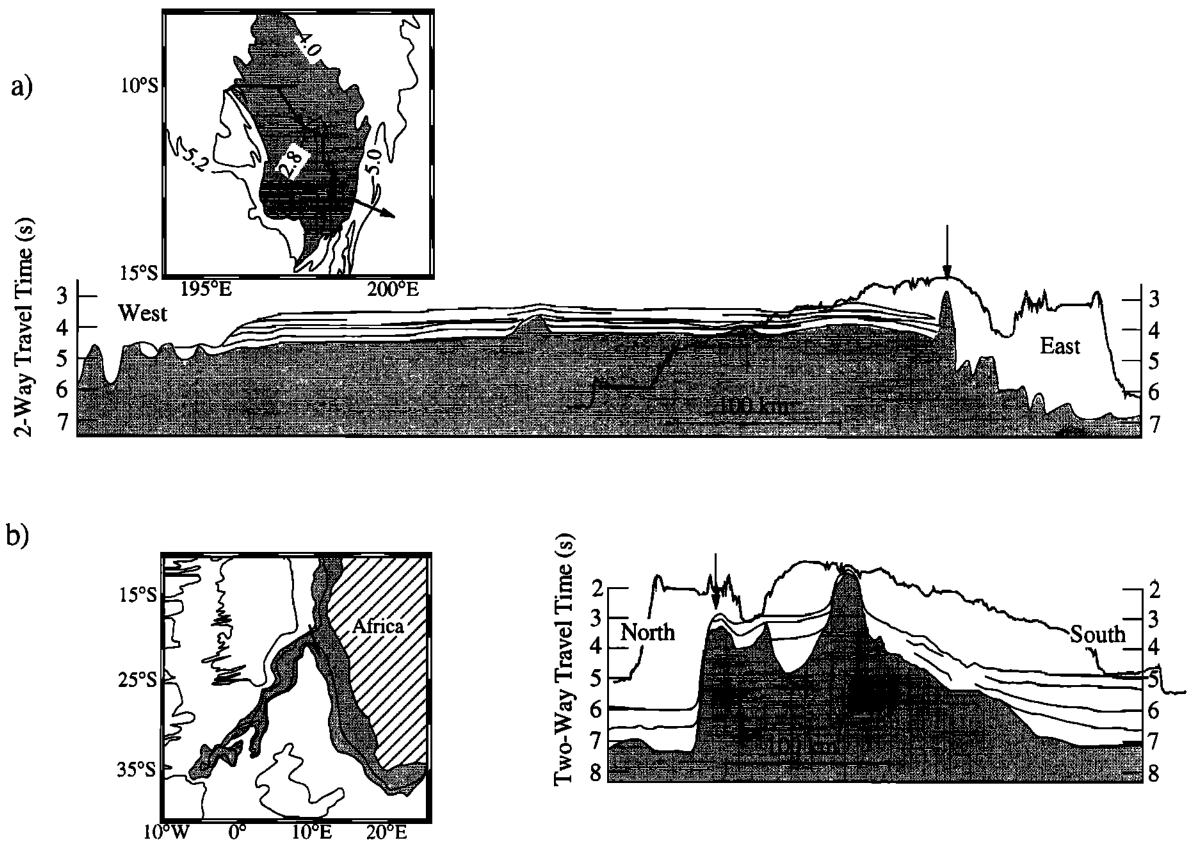

Figure 11. (a) Stratigraphic profile (from *Winterer et al.* [1974]) of the Manihiki Plateau along the ship track marked by arrows in the adjacent map (the direction of the arrows denote left-to-right in the profile). The plateau sedimentary layers are shown overlying volcanic basement (gray-shaded). Note the volcanic mounds composing the east (marked by the arrow) and west margins resemble volcanic mounds of the Tuamotu Plateau. The seafloor of the Tuamotu platform (shaded profile) is shown at the same horizontal and vertical scale for comparison. (b) Stratigraphic profile of the Walvis Ridge along the profile marked by the arrow in the adjacent map (1-km contour interval with depths shallower than 4 km shaded), drawn at the same horizontal and vertical scale as the Manihiki profile. Again the volcanic basement is gray-shaded, the overlying sediment layers are marked, and the seafloor of the Tuamotu platform is shown at the same scale. The arrows above the profiles mark the northern marginal ridge.

zone, as proposed for the Walvis Ridge, since the lineaments of the Tuamotu volcanic ridges, and the overall platform trend, are oblique to the nearby Marquesas and Austral fracture zones. Still, the plateau lineament does not directly reflect the motion of the Pacific plate over the Tuamotu hotspot, since (assuming this hotspot was stationary with respect to the Hawaiian hotspot) the change in Pacific plate motion at ~42 Ma [*Duncan and Clague*, 1985; *Lonsdale*, 1988] is not recorded in the Tuamotu lineament.

A plausible tectonic mechanism that would leave a lithospheric imprint along the Tuamotu lineament is a southward propagating segment of the Pacific-Farallon spreading center. Analogous to the Galapagos propagating rift tip near 95.5°W [*Hey et al.* 1986], the possible Tuamotu propagator may have generated an inner pseudofault (the boundary between crust generated at the northern ridge segment and that at the southern) and a failed rift zone (the lineation of the failed southern spreading segment, Figure 12). These two boundaries would enclose a block of lithosphere transferred from the Farallon plate to the Pacific plate called the "lithospheric transfer zone" by *Hey et al.* [1986]. The inner pseudofault, the failed rift zone, and the lithospheric transfer zone may have been weaknesses in the crust and lithosphere sufficient to channel hotspot melts, thereby generating the linear volcanic ridges of the plateau and hiding the change in Pacific plate motion at 42 Ma. Outside of this lithospheric transfer zone, regions such as the basin in region C may have experienced less volcanism owing to the more competent unscarred lithosphere.

Lithospheric and crustal control on volcanic morphology is discussed by *Vogt and Johnson* [1975], who show that plate boundaries such as transform faults can channel hotspot-derived magma to form ridge like edifices. Examples of such volcanic ridges are along the Clipperton, Galapagos, and Marquesas fracture zones. These ridges are thought to mark the relative motion of the Marquesas hotspot as it passed beneath the lithospheric discontinuities at these fracture zones [*McNutt et al.*, 1989]. According to *Epp* [1984], lineaments in the Hawaiian and Musician Island chains deviate from hotspot traces in response to lithospheric zones of weakness such as fracture zones. Direct evidence for channelling of hotspot material toward lithospheric discontinuities is the isotopic and trace element enrichments found along midocean ridge segments located near hotspots [*Schilling*, 1985; *Schilling et al.*, 1985]. These enrichments

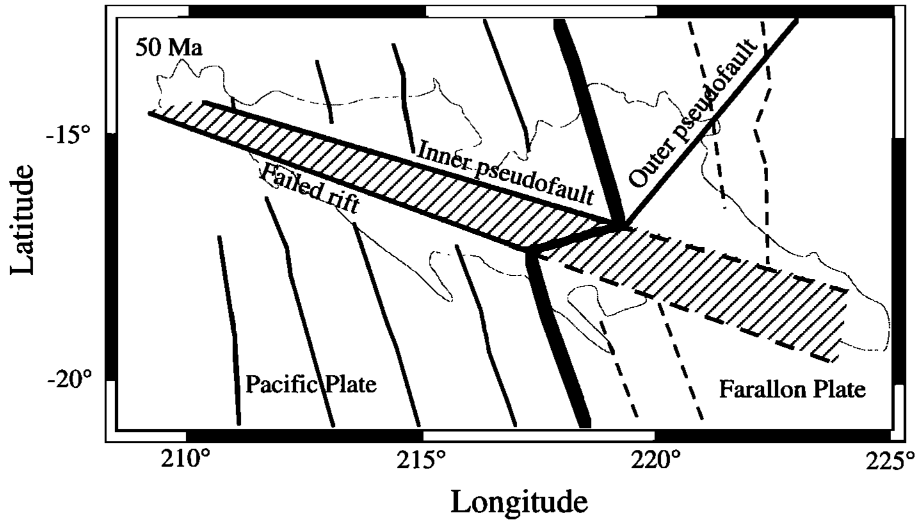

Figure 12. This cartoon illustrates the geometry of the Pacific-Farallon spreading center (thickest lines) at time 50 Ma. Isochrons (extrapolated to inferred plate boundaries) with ages greater than 50 Ma are solid, while those with ages less than 50 Ma are dashed. Our preferred model that the northern ridge segment propagated southward at the expense of the southern segment predicts a zone of lithosphere transferred from the Farallon plate to the Pacific plate (hachured) bounded to the north by the inner pseudofault and to the south by the failed rift zone. These discontinuities in the lithosphere may have focused volcanism along the Tuamotu Plateau (outlined with the 3.5-km depth contour) and shape its plateau like morphology.

indicate that hotspot material may deviate laterally from the hotspot center by as much as 800 km as a consequence, at least in part, of the thinned lithosphere at midocean ridges.

The most direct evidence for a lithospheric suture zone delineating the path of a propagating rift tip of the Pacific-Farallon spreading center is seen in the regional magnetic isochron pattern (Figure 10). The magnetization pattern reveals an age offset between crust on the southwest and northwest of the platform; and beginning with anomaly 20, the isochrons north of the plateau lengthen to the south with decreasing age, indicating that the northern segment was propagating southward when these isochrons were formed. This is the same propagating rift that *Okal and Cazenave* [1985] suggest in their model for the formation of the southeastern end of the Tuamotu platform. While the magnetic data show clear evidence for an offset between the northern and southern ridge segments, whether the northern segment was propagating before the time of anomaly 20 is less certain. The propagating rift model, however, is most attractive in that it may explain the morphology and geographic trend of the Tuamotu Plateau. Thus, while the mantle source that gave rise to the Tuamotu Plateau is most akin to the hotspots of island chains, the morphology of the plateau appears to be structurally controlled by the lithosphere, similar to other oceanic plateaus.

As for the hotspots which formed the Tuamotu platform, one possibility, is that the platform was formed by the Sala y Gomez and the Easter hotspots. As illustrated in Figure 13a the hotspot, now beneath Easter Island, may have been beneath the plateau near our survey line at 50 Ma, while the hotspot now beneath Sala y Gomez, may have been beneath the southeastern end of the Tuamotu Plateau at or near the Pacific-Farallon spreading center. The relative path of the Sala y Gomez hotspot may explain the eastward jog of the Tuamotu platform near 217°E. Additionally, as proposed by *Okal and Cazenave* [1985] another hotspot (marked X, Figure 13a) may have formed the Acteon-Oeno-Ducie seamount chain just south of the Tuamotu Plateau; however, in our model, this hotspot would have been too far west to have contributed to the Tuamotu Plateau. Our model is consistent with the model of *Okal and Cazenave* [1985] in that the Sala y Gomez hotspot would have been on axis when it generated the southeastern end of the plateau. We based our model on the rotation poles of *Duncan and Clague* [1985], which are constrained by the age progression along the Hawaiian chain. We also assume that all of the hotspots are stationary with respect to the Hawaiian hotspots.

A second possibility is based on rotation poles of *Lonsdale* [1988], which also fit the data from Hawaii, but are derived from volcanic ages along the Louisville Ridge in the Southwest Pacific Basin. In this model (Figure 13b) the Sala y Gomez hotspot may have been well east of the Tuamotu platform at ~50 Ma, while hotspot "X" would be in closer proximity to the northwestern end of the plateau. In this model, hotspot X generated the northwestern end of the plateau, while and the Easter hotspot generated the central and eastern portions. This model is consistent with the conclusions of *Woods and Okal* [1994], based on crustal structure arguments, that Sala y Gomez is not associated with the formation of the Tuamotu Plateau or its Nazca-plate conjugate, the Nazca Ridge.

If we assume hotspots are stationary with respect to each other, the models above suggest that the Tuamotu Plateau was most likely formed by two hotspots, one of which was the Easter hotspot. These hotspots liberated magma with a flux comparable to those of the Hawaiian and Marquesas hotspots, but substantially less than those that gave rise to the flood basalts of other oceanic plateaus.

Conclusions

We have developed a scenario for the formation of the northwestern end of the Tuamotu Plateau. The volcanic

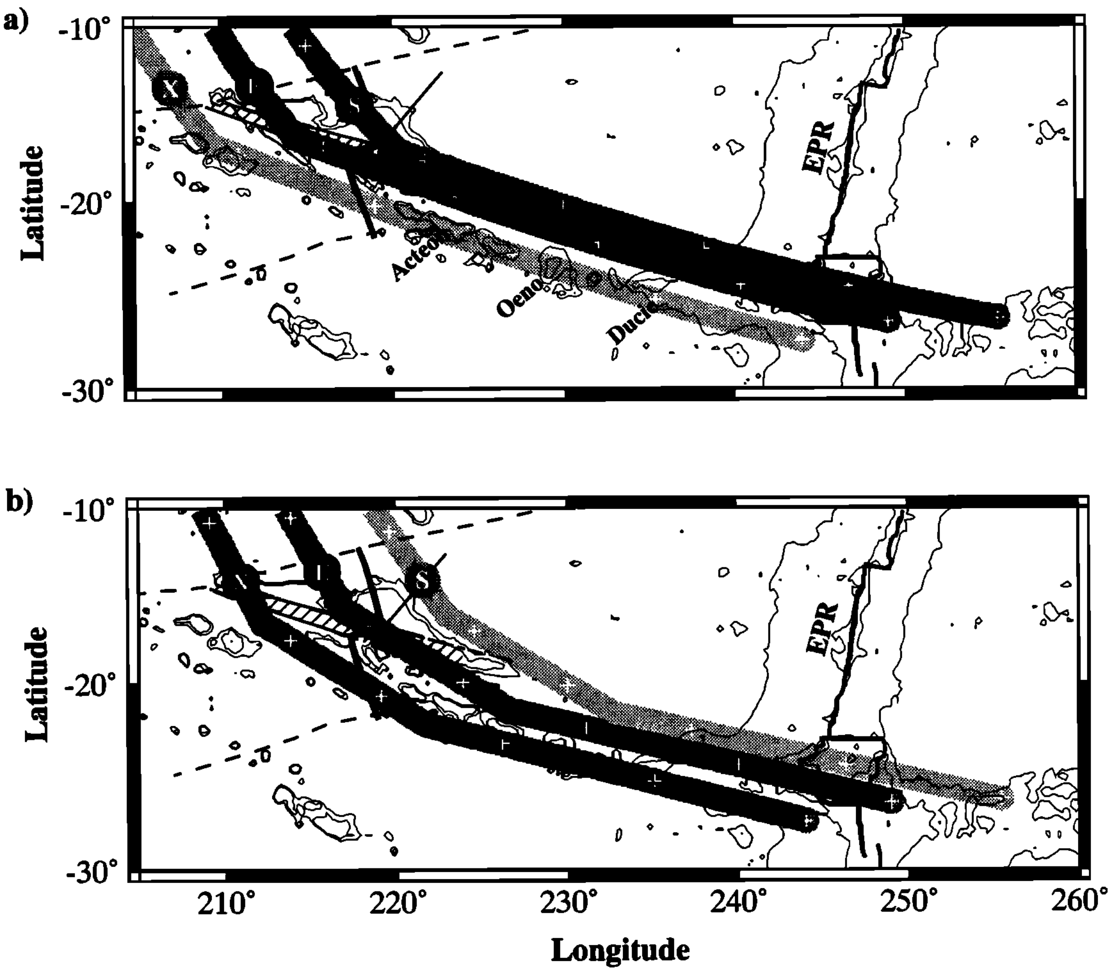

Figure 13. The configuration of the Pacific-Farallon spreading center at 50 Ma is shown as the thickest solid lines. The large dots mark the locations of the Sala y Gomez hotspot (S), the Easter hotspot (E), and the unknown hotspot (X, suggested by *Okal and Cazenave* [1985]) at ~50 Ma derived from Pacific plate rotation poles of (a) *Duncan and Clague* [1985] and (b) *Lonsdale* [1988]. The migration path of these hotspots with respect to the Pacific plate is shown as thick shaded lines with crosses marking the locations at 10-m.y. intervals.

constructs take the form of linear, continuous ridges and scarps which bound a carbonate and volcaniclastic sediment layer with thickness 1-2 km over the central portion of the plateau. Radiometric and paleontological ages of the plateau and geomagnetic ages of the seafloor indicate that the northwestern end of the plateau formed off-axis by ~600 km, on lithosphere of age 10-20 m.y. An off-axis origin is consistent with our upper bound estimates for the elastic plate thickness of 5-10 km derived from the gravity and bathymetry data, and with the subsidence implied by isostatic removal of the plateau sediments. We attribute the formation of the northwestern end of the plateau to the Easter, and one other hotspot, which erupted magmas along the suture zone of a southward propagating rift segment of the Pacific-Farallon spreading center approximately 50 Ma. This suture zone channelled hotspot melts to shape the volcanic morphology quite differently from that of island chains formed by mantle hotspots of comparable size and strength. While the local lithospheric structure may have controlled the plateau like morphology much like other oceanic plateaus which formed near plate boundaries, the mantle source may have determined the magmatic flux which is comparable to the Hawaiian and Marquesas Island chains. This unique origin for the Tuamotu Plateau sets this hotspot feature apart from typical oceanic plateaus and island chains.

Acknowledgements. The success of the cruise EW9103 was due largely to efforts of our co-chief scientist John Mutter, as well as the onboard scientific and technical staff, and the crew of the R/V *Maurice Ewing*. We thank Nathan Bangs for the use of his semblance analysis software, Peter Buhl for his time and advice put forth in the preliminary stacking of the MCS data, and Marc Munschy for supplying the coordinates of his seafloor magnetic lineation picks. Finally, we thank Carol Raymond, Uri S. Ten Brink, and David Sandwell for their constructive reviews of this manuscript. This project was funded by NSF, grant OCE-8817764.

References

Angevine, C. L., and D. L. Turcotte, On the compensation mechanism of the Walvis Ridge, *Geophys. Res. Lett., 7,* 477-479, 1980.

Antoine, C., M. Munschy, and A. Gachon, Structure and evolution of the oceanic crust in the south of Tuamotu Islands region (South Pacific), paper presented at the *International Workshop on Intraplate Volcanism: The Polynesian Plume Province,* Papeete, Tahiti, Aug., 1993.

Berggren, W. A., D. V. Kent, J. J. Flynn, and J. A. Van Couvering, Cenozoic geochronology, *Geol. Soc. Am. Bull., 96,* 1407-1418, 1985.

Boyce, R.E., Sound velocity-density parameters of sediment and rock from DSDP drill sites 315-318 on the Line Island chain, Manihiki Plateau, and Tuamotu Ridge in the Pacific Ocean, *Initial Rep. Deep Sea Drill. Proj. 33*, 695-728, 1976.

Burckle, L. H., and T. Saito, An Eocene dredge haul from the Tuamotu Ridge, *Deep Sea Res. Short Commun., 13*, 1207-1208, 1966.

Calmant, S., and A. Cazenave, Anomalous elastic thickness of the oceanic lithosphere in the south-central Pacific, *Nature, 328*, 236-238, 1987.

Cande, S. C., and D. V. Kent, A new geomagnetic polarity time scale for the Late Cretaceous and Cenozoic, *J. Geophys. Res., 97*, 13,917-13,951, 1992.

Clague, D. A., and R. D. Jarrard, Tertiary Pacific plate motions deduced from the Hawaiian-Emperor Chain, *Geol. Soc. Am. Bull., 84*, 1135-1154, 1973.

Coffin, M. F., and O. Eldholm, Scratching the surface: Estimating dimensions of large igneous provinces, *Geology, 21*, 515-518, 1993.

Detrick, R. S., and A. B. Watts, An analysis of isostasy in the world's oceans, 3., Aseismic ridges, *J. Geophys. Res., 84*, 3637-3653, 1979.

Detrick, R. S., J. G. Sclater, and J. Theide, The subsidence of aseismic ridges, *Earth Planet. Sci. Lett., 34*, 185-196, 1977.

Duncan, R. A., and D. A. Clague, Pacific plate motion recorded by linear volcanic chains, in *The Ocean Basins and Margins*, edited by A. E. M. Nairn, F. G. Stehli, and S. Uyeda, pp. 89-121, Plenum, New York, 1985.

Duncan, R. A., and I. McDougall, Linear volcanism in French Polynesia, *J. Volcanol. Geotherm. Res., 1*, 197-227, 1976.

Epp, D. Possible perturbations to hotspot traces and implications for the origin and structure of the Line Islands, *J. Geophys. Res., 89*, 11,273-11,286, 1984.

Filmer, P. E., M. K. McNutt, and C. J. Wolfe, Elastic thickness of the lithosphere in the Marquesas and Society Islands, *J. Geophys. Res., 98*, 19,565-19,577, 1993.

Filmer, P. E., M. K. McNutt, and H. F. Webb, Volcanism and archipelagic aprons in the Marquesas and Hawaiian Islands, *Mar. Geophys. Res., 16*, 385-406, 1994.

Goslin, J., and J. C. Sibuet, Geophysical study of the easternmost Walvis Ridge, South Atlantic: Deep structure, *Geol. Soc. Am. Bull., 86*, 1713-1724, 1975.

Henderson, L. J., Motion of the Pacific plate relative to the hot spots since Jurassic and models of the oceanic plateaus of the Farallon plate, Ph.D. thesis, Northwest. Univ., Evanston, Ill., 1985.

Hey, T., M. C. Kleinrock, S. P. Miller, T. M. Atwater, and R. C. Searle, Sea Beam/Deep-Tow investigation of an active oceanic propagating rift system, Galapagos 95.5°W, *J. Geophys. Res., 91*, 3369-3393, 1986.

Jackson, E. D., and S. O. Schlanger, Regional syntheses, Line Islands Chain, Tuamotu Island Chain, and Manihiki Plateau, Central Pacific Ocean, *Initial Rep. Deep Sea Drill. Proj., 33*, 915-927, 1976.

Jarrard, R. D. and D. A. Clague, Implications of Pacific island and seamount ages for the origin of volcanic chains, *Rev. Geophys., 15*, 57-76, 1977.

Kogan, M. G., Gravity anomalies and origin of the Walvis Ridge, *J. Geophys. Res., 84*, 6019-6025, 1979.

Larner, K., R. Chambers, M. Yang, W. Lynn, and W. Wai, Coherent noise in marine seismic data, *Geophysics, 48*, 854-886, 1983.

Larson, R. L., Latest pulse of Earth: Evidence for a mid-Cretaceous superplume, *Geology, 19*, 547-550, 1991.

Le Suave, R., C. Pichocki, G. Pautot, M. Hoffert, Y. Morel, M. Voisset, S. Monti, J. Amosse, and A. Kosakevitch, Geological and mineralogical study of Co-rich ferromanganese crusts from a submerged atoll in the Tuamotu Archipelago (French Polynesia), *Mar. Geol., 87*, 227-247, 1989.

Lonsdale, P., Geography and history of the Louisville hotspot chain in the Southwest Pacific, *J. Geophys. Res., 93*, 3078-3104, 1988.

Luetgert, J. H., MacRay-interactive two-dimensional seismic raytracing for the Macintosh, *U.S. Geol. Surv. Open File Rep., 92-356*, 43 pp., 1992.

Martini, E., 9., Cretaceous to recent calcareous nannoplankton from the Central Pacific Ocean (DSDP Leg 33), *Initial Rep. Deep Sea Drill. Proj., 33*, 383-397, 1976.

McNutt, M. K., and K. Fisher, The South Pacific superswell, in *Seamounts, Islands, and Atolls, Geophys. Monogr. Ser.*, vol. 43, edited by B.H. Keating, P. Fryer, R. Batiza, and G. W. Boehlert, pp. 25-34, AGU, Washington, D. C., 1987.

McNutt, M. K., K. Fischer, S. Kruse, and J. Natland, The origin of the Marquesas fracture zone ridge and its implications for the nature of hot spots, *Earth Planet. Sci. Lett., 91*, 381-393, 1989.

Menard, H. W., and M. K. McNutt, Evidence for and consequences of thermal rejuvenation, *J. Geophys. Res., 87*, 8570-8580, 1982.

Morgan, W. J., Plate motions and deep mantle convection, *Mem. Geol. Soc. Am. 132*, 7-22, 1972.

Morgan, W. J., Hotspot tracks and the opening of the Atlantic and Indian Oceans, in *The Sea*, vol. 7, *The Oceanic Lithosphere*, edited by C. Emiliani, pp. 443-487, John Wiley, New York, 1981.

Munch, C., S. Kruse, and M. McNutt, Hydrosweep, gravity and magnetic data across an abandoned rift southeast of the Manihiki Plateau (abstract), *Eos Trans. AGU., 73* (43), Fall Meeting suppl., 585, 1992.

Munschy, M., and R. Schlich, Structure and evolution of the Kerguelen-Heard Plateau (Indian Ocean) deduced from seismic stratigraphy studies, *Mar. Geol., 76*, 131-152, 1987.

O'Connor, J. M., and R. A. Duncan, Evolution of the Walvis Ridge-Rio Grande Rise hot spot system: Implications for African and South American plate motions over plumes, *J. Geophys. Res., 95*, 17,475-17,502, 1990.

Officer, C. B. and P. C. Wuenschel, Reduction of deep sea refraction data, *Tech. Rep. 1*, Lamont Geol. Obs., Palisades, N.Y., 1951.

Okal, E. A., and R. Batiza, Hotspots: The first 25 years, in *Seamounts, Islands, and Atolls, Geophys. Monogr. Ser.*, vol. 43, edited by B. Keating and R. Batiza, pp. 1-11, AGU, Washington, D.C., 1987.

Okal, E. A., and A. Cazenave, A model for the plate tectonic evolution of the east-central Pacific based on Seasat investigations, *Earth Planet. Sci. Lett., 72*, 99-116, 1985.

Parker, R. L., The rapid calculation of potential anomalies, *Geophys. J.R. Astron. Soc., 31*, 447-485, 1973.

Richards, M. A., R. A. Duncan, and V. E. Courtillot, Flood basalts and hotspot tracks: plume heads and tails, *Science, 246*, 103-107, 1989.

Sandwell, D. T., and K. R. MacKenzie, Geoid height versus topography for oceanic plateaus and swells, *J. Geophys. Res., 94*, 7403-7418, 1989.

Schilling, J.-G., Upper mantle heterogeneities and dynamics, *Nature, 314*, 62-67, 1985.

Schilling, J.-G., G. Thompson, R. Kingsley, and S. Humphris, Hotspot-migrating ridge interaction in the South Atlantic, *Nature, 313*, 187-191, 1985.

Schlanger, S. O., and the Shipboard Scientific Party, Site 318, *Initial Rep. Deep Sea Drill. Proj. 33*, 301-338, 1976.

Schlanger, S. O., M. O. Garcia, B. H. Keating, J. J. Naughton, W. W. Sager, J. A. Haggerty, J. A. Philpotts, and R. A. Duncan, Geology and geochronology of the Line Islands, *J. Geophys. Res., 89*, 11,261-11,272, 1984.

Schubert, G., and D. T. Sandwell, Crustal volumes of continents and of oceanic and continental submarine plateaus, *Earth Planet. Sci. Lett., 92*, 234-246, 1989.

Talandier, J., and E. A. Okal, Crustal structure in the Society and Tuamotu Islands, French Polynesia, *Geophys. J.R. Astron. Soc., 88*, 499-528, 1987.

Tarduno, J. A., W. V. Sliter, L. Kroenke, M. Leckie, M. Mayer, J. J. Mahoney, R. Musgrave, M. Storey, and E. L. Winterer, Rapid formation of Ontong Java Plateau by Aptian mantle plume volcanism, *Science, 254*, 399-403, 1991.

Vogt, P. R., Volcano spacing, fractures and thickness of the lithosphere, *Earth Planet. Sci. Lett., 21*, 235-252, 1974.

Vogt, P. R., and G. L. Johnson, Transform faults and longitudinal flow below the midocean ridge, *J. Geophys. Res., 80*, 1399-1428, 1975.

Watts, A. B., An analysis of isostasy in the world's oceans, 1., Hawaiian-Emperor seamount chain, *J. Geophys. Res., 83*, 5985-6005, 1978.

Watts, A. B., J. H. Bodine, and N. M. Ribe, Observations of flexure and geological evolution of the Pacific Ocean basin, *Nature, 283*, 532-537, 1980.

Winterer, E. L., Bathymetry and regional tectonic setting of the Line Islands chain, *Initial Rep. Deep Sea Drill. Proj., 33*, 731-748, 1976.

Winterer, E. L., P. F. Lonsdale, J. L. Matthews, and B. R. Rosendahl, Structure and acoustic stratigraphy of the Manihiki Plateau, *Deep Sea Res., 21*, 793-814, 1974.

Winterer, E. L., J. H. Natland, R. J. Van Waasbergen, R. A. Duncan, M. K. McNutt, C. J. Wolfe, I. Premoli Silva, W. W. Sager, and W. V. Sliter, Cretaceous guyots in the Northwest Pacific: An overview of their geology and geophysics, in *The Mesozoic Pacific: Geology, Tectonics, and Volcanism, Geophys. Monogr. Ser.*, vol 77, edited by M. S. Pringle, W. W. Sager, and W. V. Sliter, AGU, Washington, D.C. 1993.

Wolfe, C. J., M. K. McNutt, and R. S. Detrick, The Marquesas archipelagic apron: Seismic stratigraphy and implications for volcanic growth, mass wasting, and crustal underplating, *J. Geophys. Res., 99*, 13,591-13,608, 1994.

Woods, M. T., and E. A. Okal, The structure of the Nazca ridge and Sala y Gomez seamount chain from the dispersion of Rayleigh waves, *Geophys. J. Int., 117*, 205-222, 1994.

R. L. Gibson and M. McNutt, Department of Earth, Atmospheric, and Planetary Sciences, Massachusetts Institute of Technology, Cambridge, MA 02139.

G. Ito, Department of Geology and Geophysics, Woods Hole Oceanographic Institution, Woods Hole, MA 02543 (e-mail: gito@magellan.whoi.edu)

(Received June 6, 1994; revised November 11, 1994; accepted December 29, 1994.)